Available online at www.sciencedirect.com

ScienceDirect

International Journal of Solids and Structures 45 (2008) 1570–1586

INTERNATIONAL JOURNAL OF SOLIDS AND STRUCTURES

www.elsevier.com/locate/ijsolstr

Prediction of stored energy in polycrystalline materials during cyclic loading

Paul Håkansson *, Mathias Wallin, Matti Ristinmaa

Division of Solid Mechanics, Lund University, P.O. Box 118, SE-221 00 Lund, Sweden

Received 22 January 2007; received in revised form 3 September 2007
Available online 24 October 2007

Abstract

The effect of initial texture on the stored energy is investigated. Uniaxially loaded polycrystalline materials with initial textures based on the Goss component and the Brass component are analyzed. For reference purposes a single crystal and an initial isotropic crystal orientation distribution are also analyzed. Special attention is directed at the thermomechanical behavior of polycrystalline material during cyclic loading, the temperature evolution and change in stored energy are studied. Cyclic loading of Cook's membrane is also considered. The simulations are done using a rate-dependent crystal plasticity model for large deformations formulated within a thermodynamic framework. It is shown that incorporation of the latent-hardening into the Helmholtz free energy function and use of evolution laws of appropriate form allows a thermodynamically consistent heat generation due to plastic work.

Keywords: Crystal plasticity; Heat generation; Texture

1. Introduction

The properties of metals and of steel are strongly affected by the manufacturing process. In many processes in which large plastic deformations occur, a large amount of heat is generated. The effect of the resulting temperature increase on the mechanical behavior of the material can be significant and cannot be neglected in an accurate model. The large plastic deformations that occur in the forming of sheet metal as well as in many other forming processes of polycrystalline material orient the grains in a particular way, resulting in a textured material. In the present study a crystal plasticity model is used for investigating heat generation in materials with differing initial texture, the evolution of their texture is also studied. Special attention is directed at heat generation associated with cyclic loading. In order to obtain a consistent heat generation and study its effects, the crystal plasticity model employed is formulated within a thermodynamic framework.

In crystal plasticity models, plastic deformation takes place in the form of slip within a discrete slip system. It is assumed, for example, that in a fcc lattice slip occurs in three possible direction in four close packed

* Corresponding author. Tel.: +46 46 222 90 92.
E-mail address: Paul.Hakansson@solid.lth.se (P. Håkansson).

0020-7683/$ - see front matter
doi:10.1016/j.ijsolstr.2007.10.009

planes. A slip itself is a manifestation of dislocation motions. An increase in dislocation density results in a decrease in the mobility of the dislocations, due to pileups and to interaction with dislocation forests and other hindrances. The decrease in dislocation mobility can be seen as a plastic hardening or an increase in slip resistance. Any given dislocation is on a microscopic level surrounded by a stress field in which energy is stored. Since the plastic flow is due to dislocations, the stored energy increases with an increase in plastic deformation. The rate of stored energy is equal to the difference between the rate of plastic work and the dissipation of energy which leads to a heat generation.

The heat generation is often measured by the fraction of plastic work dissipated as heat, which of course is also a measure of the rate of stored energy. Taylor and Quinney (1934) made early attempts to measure this quantity. They concluded that the fraction of plastic work converted to heat is a constant lying somewhere between 0.8 and 0.95. Later experiments, on the other hand, have shown that the fraction is not a constant. Oliferuk et al. (1993), for example, showed that for austenitic steel this fraction, η, varies between 0.6 and 1, depending upon the accumulated plastic strain. Rosakis et al. (2000) also showed that η can be influenced by the strain rate. Numerical studies using discrete dislocation plasticity calculations, cf. Benzerga et al. (2005) have shown that it is not only the overall dislocation density but also the distribution of dislocations that determines the stored energy level. Experimental tests by Oliferuk and Maj (2004), who studied how the pre-strain directions affects the rate of stored energy, gave similar results. Other experimental test by, for instance, Morabito et al. (2007) shows that the heat generation due to plastic work are also of importance in applications such as fatigue.

Theories that model plastic behavior from a crystallographic viewpoint have been proposed in many papers. Early proposals of models for single crystals were made by Taylor (1938), Rice (1971), Hutchinson (1976) and Peirce et al. (1983), for example. Hutchinson (1976) introduced a model for the slip rate similar to Norton's creep law, i.e. a rate-dependent crystal plasticity model. This model has been used extensively by, e.g. Peirce et al. (1983), Nemat-Nasser and Okinaka (1996), Steinmann and Stein (1996), Borg (2007) and Kuroda and Tvergaard (2007), for instance. For modeling nearly rate-independent plasticity, the model has the advantage of the slip system being involved being active all the times. Another advantage is that the numerical treatment is easier to handle than in the case of rate-independent models and of rate-dependent models in which a stress-threshold value determines whether slip takes place.

For rate-dependent crystal plasticity model based on the Norton law it is not straightforward to find a formulation that, irrespective of loading situation, fulfills the dissipation inequality and display reasonable heat generation properties. Clayton (2005) presented a model with a reasonable dissipation, but he also pointed out that special consideration has to be given to the choice of material parameters in order to avoid a negative dissipation. A possible solution of the problem, adopted by Anand (2004) is to exclude the hardening terms in the Helmholtz free energy. This will, however, imply that all plastic work is dissipated as heat, which is not in-line with experimental test.

In the present paper a rate-dependent model that satisfies the dissipation inequality for all possible sets of constitutive parameters is proposed. The model, formulated within a thermodynamic framework for large deformations is based on the flow rule proposed by Hutchinson (1976). In order to be able to study cyclic loading the flow rule is augmented by a quantity of back-stress type. In the model that Hutchinson (1970) developed the latent-hardening is considered to be of a rate form. To obtain a thermodynamically consistent formulation here, however, account has been taken of the work of Méric et al. (1991) and Busso and Cailletaud (2005), in which the latent-hardening is incorporated on a total form in the Helmholtz free energy. The evolution of the internal variables related to slip resistance here is assumed to be local for each slip system and to be of an Armstrong–Frederick type. This format turns out to be crucial for modeling the heat generation in a consistent way and also allowing it to be calibrated to experimental tests.

The capabilities of the model will be demonstrated in numerical examples. The first example concerns the uniaxial response of a polycrystal having different initial textures, special emphasis being placed on heat generation due to plastic work. Examples showing heat generation and temperature evolution during uniaxial cyclic loading are also presented. The second numerical example deals with cyclic loading of Cook's membrane. The example concerns both the mechanical response and temperature evolution. Both this example and the previous one are analyzed, adiabatic conditions being assumed to be present. The model can also be used for a fully coupled thermomechanical analysis.

2. Thermodynamic framework

The motion of particles, in a body, labeled by their positions $\boldsymbol{X} \in \Omega_0$ at $t = 0$ can be described by a unique mapping $\boldsymbol{\varphi} : \Omega_0 \times T \to \Omega \subset \mathbb{R}^3$, where T denotes the time interval and Ω the body in its current configuration. A deformation gradient $\boldsymbol{F} = \partial_{\boldsymbol{X}}\boldsymbol{\varphi}$ that maps line segments in the reference configuration to the current configuration is introduced. The change in density between the reference and the current configurations is described by $J = \det(\boldsymbol{F}) = \rho_0/\rho$. Reversible and irreversible deformation are separated from each other by the introduction of a stress-free intermediate configuration, which results in a multiplicative split of the deformation gradient, cf. Kröner (1960), Lee (1969),

$$\boldsymbol{F} = \boldsymbol{F}^{\mathrm{r}}\boldsymbol{F}^{\mathrm{p}} \tag{1}$$

The irreversible part of the deformation gradient, denoted as $\boldsymbol{F}^{\mathrm{p}}$, consists in the case of crystal plasticity of the superposition of the slip that occurs on the individual slip system. The reversible part, $\boldsymbol{F}^{\mathrm{r}}$, includes both elastic and thermal deformation according to $\boldsymbol{F}^{\mathrm{r}} = \boldsymbol{F}^{\theta}\boldsymbol{F}^{\mathrm{e}}$. The thermal deformation is assumed to be purely volumetric, i.e. $\boldsymbol{F}^{\theta} = (J^{\theta})^{1/3}\boldsymbol{1}$. Two quantities important to the establishment of constitutive relations are the spatial velocity gradient, $\boldsymbol{L}$, and the plastic velocity gradient, $\boldsymbol{l}^{\mathrm{p}}$, defined as

$$\boldsymbol{L} = \dot{\boldsymbol{F}}\boldsymbol{F}^{-1}, \qquad \boldsymbol{l}^{\mathrm{p}} = \dot{\boldsymbol{F}}^{\mathrm{p}}(\boldsymbol{F}^{\mathrm{p}})^{-1} \tag{2}$$

The second law of thermodynamics, which places formal restrictions on the constitutive model, can be formulated for continuum mechanical purposes as the dissipation inequality. Taking advantage of the fact that the dissipation inequality can be expressed in terms of the Helmholtz free energy, which without loss a of generality can be assumed to be a function of the reversible deformation tensor, $\boldsymbol{C}^{\mathrm{r}} = \boldsymbol{F}^{rT}\boldsymbol{F}^{\mathrm{r}}$, of the temperature and of a collection of internal variables used to characterize the dislocation structure and the isotropic and kinematic hardening properties. The dissipation inequality can be expressed as

$$\gamma = \gamma_{\mathrm{mech}} + \gamma_{\mathrm{therm}} \geqslant 0 \tag{3}$$

where

$$\gamma_{\mathrm{mech}} = \boldsymbol{\tau} : \boldsymbol{D} - \rho_0\partial_{\boldsymbol{A}}\psi : \dot{\boldsymbol{A}} \geqslant 0 \quad \text{and} \quad \gamma_{\mathrm{therm}} = -\frac{J}{\theta}\boldsymbol{q}\cdot\partial_{\boldsymbol{x}}\theta \geqslant 0 \tag{4}$$

and where $\boldsymbol{\tau}$ and $\boldsymbol{D} \equiv \mathrm{sym}(\boldsymbol{L}) = \frac{1}{2}(\boldsymbol{L} + \boldsymbol{L}^{\mathrm{T}})$ are the Kirchhoff stress tensor and the rate of deformation tensor, respectively, $\boldsymbol{q}$ denoting the spatial heat flux vector. θ is the absolute temperature and the entropy is given by $s = -\partial_{\theta}\psi$. For notation purposes, the set $\boldsymbol{A}$ was introduced, which contains $\boldsymbol{C}^{\mathrm{r}}$ as well as the internal variables. Note that (4) provides a conservative assumption. The inner product related to $\boldsymbol{A}$, which is denoted by $(\cdot):(\cdot)$, should be regarded as a generic inner product, defined for both second-order tensors and sets of variables. The thermal part of the dissipation is always positive, due to the use of Fourier's law, whereas the mechanical dissipation, γ_{mech}, is determined by the mechanical constitutive equations. For a discussion of the derivation of the dissipation inequality the reader is referred to Håkansson et al. (2005).

The first law of thermodynamics defines an energy balance, which can be expressed in localized form in the reference configuration based on the Helmholtz free energy function, as

$$\rho_0 c\dot{\theta} = \gamma_{\mathrm{mech}} + \rho_0 r + \rho_0\theta\partial^2_{\theta\boldsymbol{A}}\psi : \dot{\boldsymbol{A}} - J\mathrm{div}(\boldsymbol{q}) \tag{5}$$

where r is an external heat source per unit volume and $\mathrm{div}(\cdot)$ denotes the spatial divergence operator. The specific heat c is introduced in (5) as $c = -\theta\partial^2_{\theta\theta}\psi$. If a coupled thermomechanical problem is to be solved, this balance law serves together with Fourier's law as the basis for the thermal finite element formulation.

3. Description of the constitutive relations

The properties of a thermodynamically consistent model are to a large extent determined by the choice of the Helmholtz free energy function. It will be assumed here that $\psi = \psi(\boldsymbol{C}^{\mathrm{r}}_i, J, g^{\alpha}, v^{\alpha}, \theta)$, where $\boldsymbol{C}^{\mathrm{r}}_i$ is the reversible isochoric deformation tensor $\boldsymbol{C}^{\mathrm{r}}_i = (J^{\mathrm{r}})^{-2/3}(\boldsymbol{F}^{\mathrm{r}})^{\mathrm{T}}\boldsymbol{F}^{\mathrm{r}}$, g^{α} are related to the slip resistance and v^{α} are quantities related to the resolved back-stress. The superscript α, which ranges from 1 to n, denotes the slip system,

where n is the total number of slip systems present in a crystal. It is assumed that the free energy can be split into a reversible part, related to the elastic and the thermal state, and an irreversible part ψ^{p}, which is related to the slip mechanisms, i.e.

$$\rho_0\psi(\boldsymbol{C}_i^{\mathrm{r}}, J, g^\alpha, v^\alpha, \theta) = \rho_0\psi^{\mathrm{r}}(\boldsymbol{C}_i^{\mathrm{r}}, J, \theta) + \rho_0\psi^{\mathrm{p}}(g^\alpha, v^\alpha) \tag{6}$$

The reversible part of the free energy is assumed to be described by

$$\rho_0\psi^{\mathrm{r}}(\boldsymbol{C}_i^{\mathrm{r}}, J, \theta) = K\left[\frac{1}{2}(\ln J)^2 - 3\alpha\Delta\theta\ln J\right] + 2GJ_2^{\mathrm{r}} + \rho_0 c\left[\Delta\theta - \theta\ln\left(\frac{\theta}{\theta_0}\right)\right] \tag{7}$$

where $\Delta\theta$ is the difference between the current temperature, θ, and the reference temperature, θ_0. The invariant J_2^{r} is calculated from the right stretch tensor $\boldsymbol{U}^{\mathrm{r}} = \sqrt{\boldsymbol{C}^{\mathrm{r}}}$ as

$$J_2^{\mathrm{r}} = \frac{1}{2}\mathrm{tr}[(\ln \boldsymbol{U}^{\mathrm{r}})^{\mathrm{dev}}(\ln \boldsymbol{U}^{\mathrm{r}})^{\mathrm{dev}}] \tag{8}$$

where the superscript dev denotes the deviatoric part. In (7) the material parameters K and G represent the initial bulk modulus and the shear modulus, respectively. The thermal expansion coefficient α is assumed to be independent of the temperature. The parameter c in (7) can be identified as the specific heat. Using that the Kirchhoff stress tensor is defined as

$$\boldsymbol{\tau} = 2\rho_0\boldsymbol{F}^{\mathrm{r}}\partial_{\boldsymbol{C}^{\mathrm{r}}}\psi(\boldsymbol{F}^{\mathrm{r}})^{\mathrm{T}} \tag{9}$$

it follows, by insertion of (7) into (4), that

$$\gamma_{\mathrm{mech}} = \boldsymbol{\Sigma} : \boldsymbol{l}^{\mathrm{p}} - \sum_{\alpha=1}^{n}(G^\alpha\dot{g}^\alpha + b^\alpha\dot{v}^\alpha) \tag{10}$$

where use being made of the definition the Mandel stress tensor

$$\boldsymbol{\Sigma} = 2\rho_0\boldsymbol{C}^{\mathrm{r}}\partial_{\boldsymbol{C}^{\mathrm{r}}}\psi \tag{11}$$

In (10) the following definitions were also introduced:

$$G^\alpha = \rho_0\partial_{g^\alpha}\psi \quad \text{and} \quad b^\alpha = \rho_0\partial_{v^\alpha}\psi \tag{12}$$

In crystal plasticity models the plastic deformation takes place on specific slip planes. For a fcc lattice, the slip occurs on the four close packed planes, each having three slip directions, slip in the $\{1\,1\,1\}\langle\bar{1}\,0\,1\rangle$ systems thus being allowed. On a macroscopic scale, plastic evolution is governed by $\boldsymbol{l}^{\mathrm{p}}$, which is formed as the sum of the shear rate in all slip systems, cf. Rice (1971)

$$\boldsymbol{l}^{\mathrm{p}} = \sum_{\alpha=1}^{n}\dot{\gamma}^\alpha\boldsymbol{M}^\alpha \otimes \boldsymbol{N}^\alpha \tag{13}$$

The slip direction $\boldsymbol{M}^\alpha$ and the normal vector of the slip plane $\boldsymbol{N}^\alpha$ are defined in the intermediate configuration and can be mapped to the current configuration via $\boldsymbol{m}^\alpha = \boldsymbol{F}^{\mathrm{r}}\boldsymbol{M}^\alpha$ and $\boldsymbol{n}^\alpha = (\boldsymbol{F}^{\mathrm{r}})^{-\mathrm{T}}\boldsymbol{N}^\alpha$. The orientation of the slip direction and of the slip plane in the intermediate configuration is assumed to be coherent with the orientation of the continuum in the reference configuration, which implies that the intermediate configuration is an isoclinic configuration, cf. Mandel (1971). The non-uniqueness of the intermediate configuration is thereby eliminated. Note that the evolution law (13) implies that $\mathrm{tr}(\boldsymbol{l}^{\mathrm{p}}) = 0$, which as a consequence implies that $J^{\mathrm{p}} = 1$, plastic incompressibility thus being adopted.

Use of the slip direction and vector normal to the slip plane above allows the resolved shear stress, i.e. the Schmid stress, in the intermediate configuration to be defined as

$$\tau^\alpha = \boldsymbol{M}^\alpha\boldsymbol{\Sigma}\boldsymbol{N}^\alpha \tag{14}$$

The slip rate $\dot{\gamma}^\alpha$ is modeled by a power law, such that

$$\dot{\gamma}^\alpha = \dot{\gamma}_0\left(\frac{|\tau^\alpha - b^\alpha|}{G_r^\alpha}\right)^m \mathrm{sgn}(\tau^\alpha - b^\alpha) \tag{15}$$

The parameters $\dot{\gamma}_0$ and m are the reference slip rate and the rate sensitivity, respectively. The resolved back-stress, b^α, is due to directional resistance of dislocation movements on slip system level. The directional resistance originates from long-range stresses due to heterogeneous dislocation structures, for instance, in form of dislocation pile-ups in the neighborhood of precipitates, grain boundaries and other dislocation obstacles. At a macroscopic level the back-stress result in the well known Bauchinger effect. The slip resistance or shear strength G_r^α consists of two parts. The first part G_0 reflects the lattice friction, cf. Ohashi (2004), and is constant for all slip system. The second part G^α reflects the resistance for dislocation movements due to short-range interaction between dislocations. The resistance due to the dislocation structure can evolve differently on different slip system, hence the superscript α denoting the slip system. The evolution of G^α is in general dependent on activity on other slip system. The form for the slip resistance G_r^α adopted here is taken as

$$G_r^\alpha = G_0\left(\frac{\theta_0}{\theta}\right)^{p_1} + G^\alpha\left(\frac{\theta_0}{\theta}\right)^{p_2} \tag{16}$$

The temperature dependence incorporated into the model is due to a reduced lattice friction and an increase in dislocation mobility at higher temperatures, which at a macroscopic level results in thermal softening. In the general situation the temperature dependence of the lattice friction and the dislocation mobility differs and consequently the parameters p_1 and p_2 as well as the reference temperature θ_0 are introduced to control the temperature dependence.

Extensive experimental and numerical studies of the evolution of slip resistance when multiple slip occurs have been conducted. The slip resistance on one slip system is known to be highly dependent on the slip on the other systems involved, resulting in latent-hardening or cross-hardening. For many materials, the latent-hardening is considerably stronger than the self-hardening, i.e. the hardening which appears on a slip system due to slip on the same system, it is thus important to incorporate the latent-hardening into the model. For a detailed discussion of latent-hardening, see Hill, 1966; Hutchinson, 1970; Peirce et al., 1982. Here, the latent-hardening is incorporated into the model via the Helmholtz free energy. The internal variable g^α is a measure of the local slip plane resistance. The hardening is, however, not independent on the hardening on neighboring slip planes and consequently the stored energy, due to the dislocation structure must dependent on individual g^α but also the coupled terms. A simple quadratic format for the irreversible part of the free energy, previously used by Méric et al. (1991) and Busso and Cailletaud (2005), is adopted

$$\rho_0\psi^{\mathrm{p}} = \frac{1}{2}H\sum_{\alpha=1}^{n}(v^\alpha)^2 + \frac{1}{2}Q\sum_{\alpha=1}^{n}\sum_{\beta=1}^{n}h_{\alpha\beta}g^\alpha g^\beta \tag{17}$$

where H and Q are material parameters. The hardening matrix $h_{\alpha\beta} = \delta_{\alpha\beta} + q(1-\delta_{\alpha\beta})$ is in line with the format proposed by Hutchinson (1970). The parameter q controls the ratio between the self-hardening and the latent-hardening. An increased q will on a macroscopic level result in an increased hardening due to the latent-hardening. On a microscopic level the value of q will at a prescribed deformation affect the slip on the various slip systems. If q is set to 1, the latent-hardening is equal to the self-hardening. Experiment performed on fcc-metals indicates that the latent hardening is stronger than the self-hardening, i.e. $q > 1$, see for instance Franciosi, 1985; Piercy et al., 1955. The free energy (17) together with (12) results in the following slip resistance and back stress:

$$G^\alpha = Q\sum_{\beta=1}^{n}h_{\alpha\beta}g^\beta \qquad \text{and} \qquad b^\alpha = Hv^\alpha \tag{18}$$

To complete the theory, evolution laws for g^α and v^α are also needed. An evolution law for v^α similar to that of Armstrong–Frederick, cf. e.g. Horstemeyer et al. (1999), is used

$$\dot{v}^\alpha = \dot{\gamma}^\alpha - Rv^\alpha|\dot{\gamma}^\alpha| \tag{19}$$

where R is a parameter controlling the saturation of v^α. The second term in (19) is often referred to as a dynamic recovery term. The evolution law (19) together with (12) determine the back-stress b^α. The evolution law for g^α is similar to the evolution law for v^α in (19), i.e. it is local for each slip system. In line with Steinmann

and Stein (1996), it is assumed here that the evolution for g^α in addition to $\dot{\gamma}^\alpha$ also depends on the ratio $|\tau^\alpha - b^\alpha|/G_r^\alpha$, i.e.

$$\dot{g}^\alpha = (1 - Bg^\alpha)\frac{|\tau^\alpha - b^\alpha|}{G_r^\alpha}|\dot{\gamma}^\alpha| \tag{20}$$

The evolution law (20) exhibits a saturation of the hardening due to saturation of the dislocation density, where B is a material parameter controlling the saturation value of g^α. An Armstrong–Frederick type evolution law for the slip resistance has been used by numerous authors, for instance Horstemeyer et al. (1999) and Clayton (2005), although (20) differs in its being local for each slip system and in $\dot{g}^\alpha$ being driven by $|\tau^\alpha - b^\alpha|/G_r^\alpha|\dot{\gamma}^\alpha|$ instead of simply be $|\dot{\gamma}^\alpha|$. The consequence of the term $|\tau^\alpha - b^\alpha|/G_r^\alpha$ being present in (20) is that $\dot{g}^\alpha$ is reduced for stress states where $|\tau^\alpha - b^\alpha|$ is smaller than G_r^α. In the case of nearly rate-independent plasticity, i.e. when $m \to \infty$ in (15), the term $|\tau^\alpha - b^\alpha|/G_r^\alpha \to 1$. This choice of evolution law is very similar to the hardening law proposed by Bodner and Partom (1975), in which plastic work is used as the state variable for the hardening.

An expression for the mechanical dissipation can be derived through the evolution laws (19) and (20) together with (15) and (14) being inserted in (10)

$$\gamma_{\text{mech}} = \sum_{\alpha=1}^{n}\left(|\tau^\alpha - b^\alpha| - \frac{|\tau^\alpha - b^\alpha|}{G_r^\alpha}G^\alpha + B\frac{|\tau^\alpha - b^\alpha|}{G_r^\alpha}G^\alpha g^\alpha + \frac{H}{R}(b^\alpha)^2\right)|\dot{\gamma}^\alpha| \tag{21}$$

It can be concluded that the mechanical dissipation is always positive. The last two terms are individually positive, since both G^α and g^α are positive, and the second term is always smaller than the first term. It is obvious from (21) that if the term $|\tau^\alpha - b^\alpha|/G_r^\alpha$ is absent in (20) a loading situation in which the dissipation becomes negative can easily arise. During cyclic loading, for example, the quantity $|\tau^\alpha - b^\alpha|$ can be zero at the same as G^α is larger than zero due to hardening.

4. Results

The characteristic features of the model will be demonstrated by considering a polycrystalline material. There are several different methods for modeling polycrystal behavior based on constitutive models for single crystals. The scheme introduced by Taylor (1938), in which it is assumed that all the crystals in an aggregate are subjected to the same deformation, is used here. Although the compatibility between the grains in the aggregate is fulfilled with use of the scheme, equilibrium over grain boundaries is generally not satisfied. The Taylor assumption generally predicts the mechanical response and the texture evolution quite well, cf. Miehe et al. (1998), Anand et al. (1997). However, the Taylor assumption has the disadvantage of being kinematically overconstrained resulting, in a too stiff response, which in some situations causes the texture to evolve too fast. The major advantages of the Taylor assumption as compared with other, more accurate methods are its simplicity and its computational efficiency. In the average scheme, the deformation gradient and the rate of deformation in all the grains are equal. Since the rate of mechanical energy integrated over all of the grains should be equal to the macroscopic rate of energy in the aggregate, the macroscopic Kirchhoff stress tensor is obtained as an average over all of the grains, i.e.

$$\boldsymbol{\tau} = \frac{1}{n}\sum_{i=1}^{n}\boldsymbol{\tau}^i \tag{22}$$

where n is the total number of grains in the aggregate and $\boldsymbol{\tau}^i$ is the Kirchhoff stress tensor in an individual grain. Under adiabatic conditions the homogenized temperature, θ, is obtained from the energy balance as

$$\theta = \frac{1}{n}\sum_{i=1}^{n}\theta^i \tag{23}$$

The integration scheme for the constitutive equations for a single crystal is given in the Appendix. The macroscopic quantities can be obtained then using (22) and (23).

The material parameters are chosen to mimic the thermal and mechanical response of polycrystalline austenitic steel, where it is assumed that slip can take place on the 12 slip systems $\{1\,1\,1\}\langle\bar{1}\,0\,1\rangle$. Furthermore, the simulations are performed under adiabatic conditions. The elastic parameters, i.e. the initial shear modulus and the bulk modulus, are taken as $G = 80$ MPa and $K = 164$ MPa, respectively. The thermal expansion coefficient is $\alpha = 1 \cdot 10^{-5}\ \mathrm{K}^{-1}$ and the density is set to $\rho_0 = 7800\ \mathrm{kg/m^3}$. The heat capacity is $c = 450$ J/kg K and the reference temperature θ_0 is set to 293 K.

Since dislocations are present in virgin material, the internal variable g^α is not zero initially, i.e. $g^\alpha(t=0) = g_0^\alpha \neq 0$. The parameters related to the hardening are taken as follows:

$$\begin{aligned} &H = 650\ \mathrm{MPa}, \quad R = 10, \quad Q = 200\ \mathrm{MPa} \\ &B = 8, \quad g_0^\alpha = 7 \times 10^{-3}, \quad G_0 = 55\ \mathrm{MPa} \end{aligned} \tag{24}$$

This choice of material parameters gives an uniaxial mechanical behavior that agrees well with the experimental test performed by Oliferuk et al. (1993) on austenitic steel. In accordance with Peirce et al. (1982) the parameter related to the latent-hardening is taken as $q = 1.4$. This parameter is, however, not necessarily constant. Franciosi (1985) has, for instance, shown that for many fcc-metals the parameter is highly dependent on the accumulated slip and it may take values both larger than 1 as well as smaller than 1. For steel the value 1.4 is a reasonable approximation.

Although the strain-rate dependence is small, for high loading rates it cannot be neglected. The choices of $m = 26$ and $\dot{\gamma}_0 = 1 \times 10^{-3}$ are made to be in line the experimental data reported by Andrade-Campos et al. (2005) and Chen et al. (2004). The influence of the temperature on the slip resistance is determined by the parameters p_1 and p_2 in (15). The choice of $p_1 = 0.7$ and $p_2 = 0.7$ results in thermal behavior that agrees with the experimental findings for austenitic steel reported in Tavassoli (1995). Generally the temperature dependences of the lattice friction and the dislocation mobility are not equal, but in order to simplify the calibration it is assumed that the temperature dependence is equal.

4.1. Uniaxial loading

The uniaxial examples in this section aim to show how different initial crystal orientation distributions influence the mechanical response and the heat generation due to plastic work. The evolution of temperature and texture are also studied. A fully integrated 3D isoparametric element having 400 grains at each integration point is used in the simulations. The material is loaded with a constant logarithmic strain rate of $0.1\ \mathrm{s}^{-1}$ in the rolling direction (RD). The boundary conditions are applied in such a way that a uniaxial stress state is obtained, the only non-vanishing stress component being σ_{11}.

In a comparison of models with experimental results it is suitable to assess the heat generation in terms of the fraction of the plastic work dissipated as heat, i.e.

$$\eta = \frac{\gamma_{\mathrm{mech}}}{w^{\mathrm{p}}} \tag{25}$$

In (25), the mechanical dissipation is derived in (21) and the rate of plastic work is defined as $w^{\mathrm{p}} = \sum_{\alpha=1}^{n} \tau^\alpha \dot{\gamma}^\alpha$. In an experimental test, the dissipation cannot be measured directly, but the fraction of plastic work dissipated as heat can be calculated using the heat equation (5). If adiabatic conditions are assumed, η can, from experimental measurements, be calculated as

$$\eta = \frac{\rho_0 c \dot{\theta}}{w^{\mathrm{p}}} \tag{26}$$

Figs. 1–3 show the mechanical and the thermal response in uniaxial loading for a polycrystalline material with an initial isotropic orientation distribution, see the pole figure in Fig. 3a). The pole figures are of the so-called equal-area mapping type, cf. Kocks et al. (1998), and all the texture plots are $\{1\,1\,1\}$-pole figures. The rolling direction, RD, and the transverse direction, TD, are marked in the pole figures, whereas the normal direction, ND, is not marked but is located in the center of the figures. The mechanical response is shown in Fig. 1, the response obtained for an isothermal analysis is also presented for reference purposes.

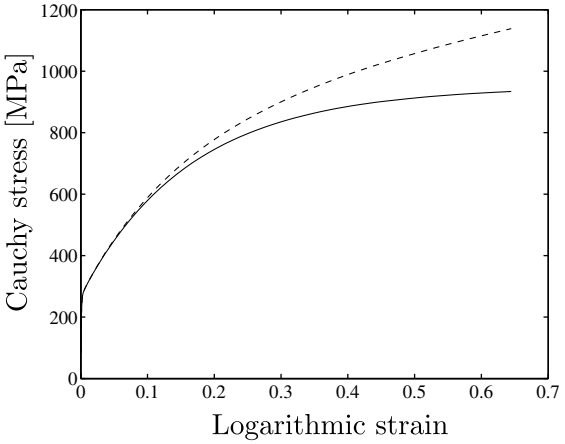

Fig. 1. The uniaxial mechanical responses obtained for a polycrystal model with an initially isotropic distribution of the crystal orientations. The result of an adiabatic analysis is shown by the solid line and of an isothermal analysis by the dashed line.

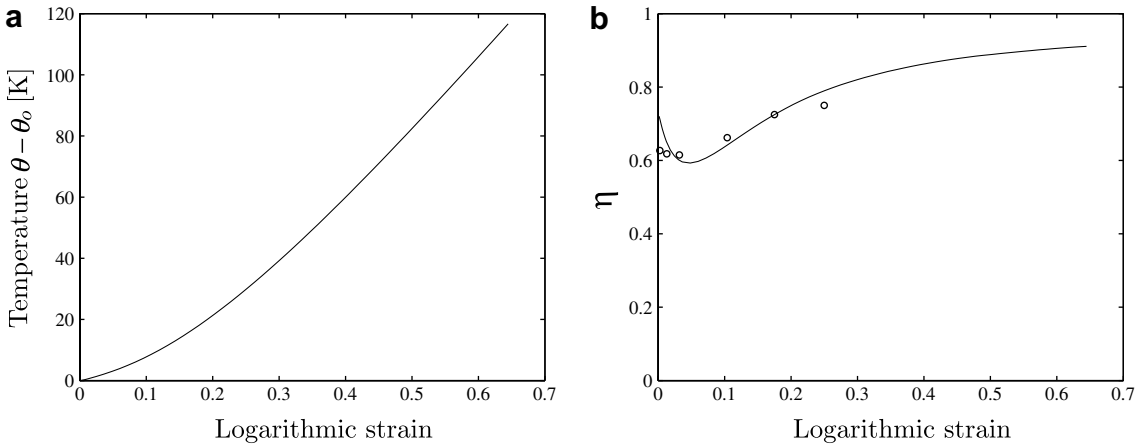

Fig. 2. Uniaxial thermal response of a polycrystal model having an initially isotropic distribution of the crystal orientations: (a) temperature evolution, (b) η, the fraction of plastic work dissipated as heat. The circles represent experimental data from Oliferuk et al. (1993).

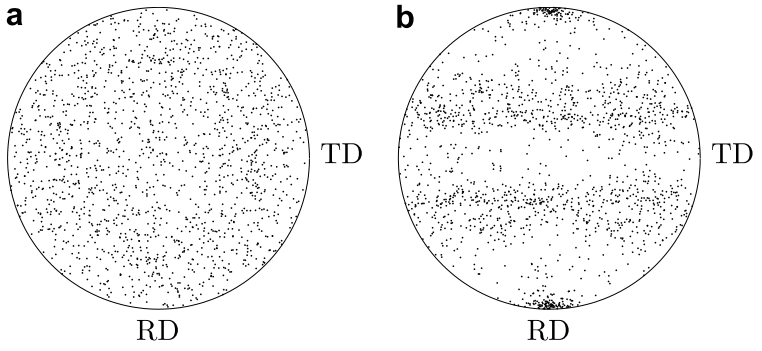

Fig. 3. {1 1 1}-pole figures of the texture evolution in a polycrystal model having an initially isotropic distribution of crystal orientations: (a) initial texture, (b) texture at a logarithmic strain of 0.65.

The temperature evolution and the variation in the fraction of plastic work dissipated as heat are shown in Fig. 2. The characteristics and magnitude of the η-factor in Fig. 2b agree qualitatively well with the experimental findings for austenitic steel of Oliferuk et al. (1993). See also the discussion in Ristinmaa et al. (2007).

The texture developed is shown in Fig. 3b. As expected, the initially randomly distributed {1 1 1}-poles move in the RD-direction on the lower and the upper side of the pole figure and towards two equally distributed horizontal bands. The texture developed in the isothermal case, not shown, is almost identical to the texture in the adiabatic case shown in Fig. 3b). The reason for this can be found in the evolution law for $\boldsymbol{l}^{\mathrm{p}}$, cf. (13). Since the orientation of the stress tensor is insensitive to the temperature evolution, the plastic rotation for a given deformation is almost independent of the temperature change.

Analyzes of uniaxial loading were also performed on aggregates with two different anisotropic initial crystal orientation distributions. The first distribution is based on randomly generated orientations around the Goss component. The Goss orientation is obtained from the Euler angles $\psi_1 = 0°$, $\Theta = 45°$ and $\psi_2 = 0°$ according to the Bunge system, cf. Kocks et al. (1998). The global coordinate system is oriented in such a way that the x-axis is parallel to the RD-direction and the z-axis is parallel to the ND-direction. The method of obtaining a randomized distortion around the specific orientation follows Kuroda and Tvergaard (2007), where each grain is rotated around a direction that is randomly selected. The randomized choice of direction follows a rectangular distribution, whereas the rotation, having a standard deviation of 15°, follows a Gaussian distribution. The initial distribution is shown in Fig. 4a. During uniaxial loading in the RD-direction, the orientation of the crystals evolves towards an orientation in which the [1 0 0] direction aligns with the loading direction and the [0 1 0] direction aligns with the transverse directions. This orientation is the same as the initial Goss orientation. The loading thus results in a concentration of the poles, cf. Fig. 4.

The next initial crystal distribution to be considered is a distribution based on the Brass component, which is an orientation that is often dominant after the rolling of sheet metals. The orientation component is described by the Euler angles $\psi_1 = 35°$, $\Theta = 45°$ and $\psi_2 = 0°$. The randomized distortion around the Brass orientation is generated in the same way as for the Goss distribution. The initial texture is shown in Fig. 5a and the final texture, at a logarithmic strain of 0.65, in Fig. 5b. The reorientation of the grains results in a texture with characteristics close to those obtained when using an initial isotropic distribution, see Fig. 3b. The texture shown in Fig. 3b, at the same deformation level is not equally pronounced, however.

The texture developed in the case of the Brass distribution is characterized by a rotation of the crystals in such a way that the vectors normal to the {1 1 1} planes moves towards the loading direction. The difference between the textures developed from the Brass distribution and the isotropic distribution stems from the initial rotation of the crystals around the loading direction (RD). Since the loading is uniaxial, the change in rotation is limited, as can be seen in Fig. 5b).

The mechanical response obtained for the distributions based on the Goss orientation and the Brass orientation are presented in Fig. 6. For reference purposes, the response of a single crystal oriented such that the crystallographic axes are aligned with the RD, TD and ND directions is presented as well. Since the [1 0 0] direction is aligned with the loading direction for both the single crystal and the Goss distribution, the differ-

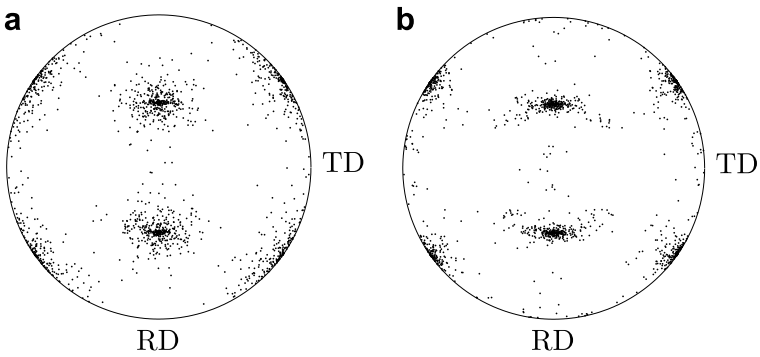

Fig. 4. {1 1 1}-pole figures of the texture evolution in a polycrystal model having an initial crystal distribution around the Goss component: (a) initial texture, (b) texture at a logarithmic strain of 0.65.

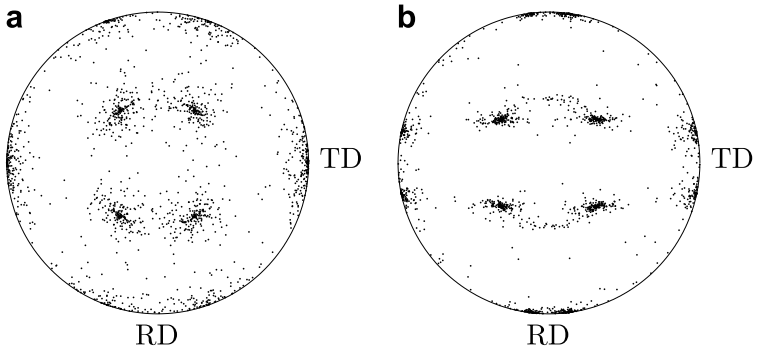

Fig. 5. {1 1 1}-pole figures of texture evolution for a polycrystal model with an initial crystal distribution around the Brass component: (a) initial texture, (b) texture at a logarithmic strain of 0.65.

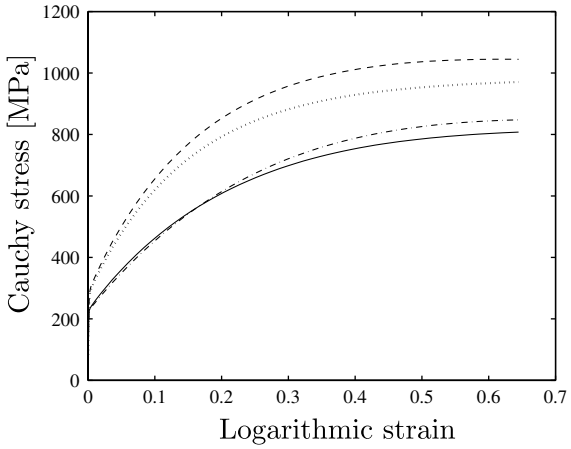

Fig. 6. Uniaxial mechanical response for different distributions of the crystal orientations. Goss distribution – solid line, Brass distribution – dashed line, single crystal – dashed-dotted line, isotropic distribution – dotted line.

ence in mechanical responses between the Goss distribution and the single crystal is due to the scatter around the Goss orientation. It can also be concluded that the Brass distribution yields a behavior that is considerably stiffer than that of the single crystal as well as the Goss distributions and the isotropic distribution. It is no surprise that the temperature evolutions in Fig. 7a follow a pattern similar to that of the mechanical response. The clearest differences between the various initial distributions can be found in the relation between the rate of stored energy and the rate of plastic work, as shown in Fig. 7b in the form of the η-factor. The single crystal is loaded in the [1 0 0] direction yielding identical slip, and thus identical hardening too, for all the slip systems except for the four slip systems with slip directions perpendicular to the loading direction, the slip on each of these four other slip systems are zero. For the Goss distribution, in which the specific Goss orientation component coincides with the loading direction, the randomized distortion yields slip and hardening that differ for the various slip systems. This non-uniform hardening results in a lower rate of stored energy. As the dispersion of the crystal orientations increases, the η-factor approaches the η-factor in the case of the initially isotropic crystal orientation distribution. Note that the η-factor for the Brass distribution, in which there is a significant reorientation of the crystals, is close to the η-factor for the isotropic distribution.

4.2. Cyclic uniaxial loading

Special attention is given the cyclic loading since the heat generation due to plastic work can give rise to significant temperature increases, even for moderate strain amplitudes. The first analysis is based on the same

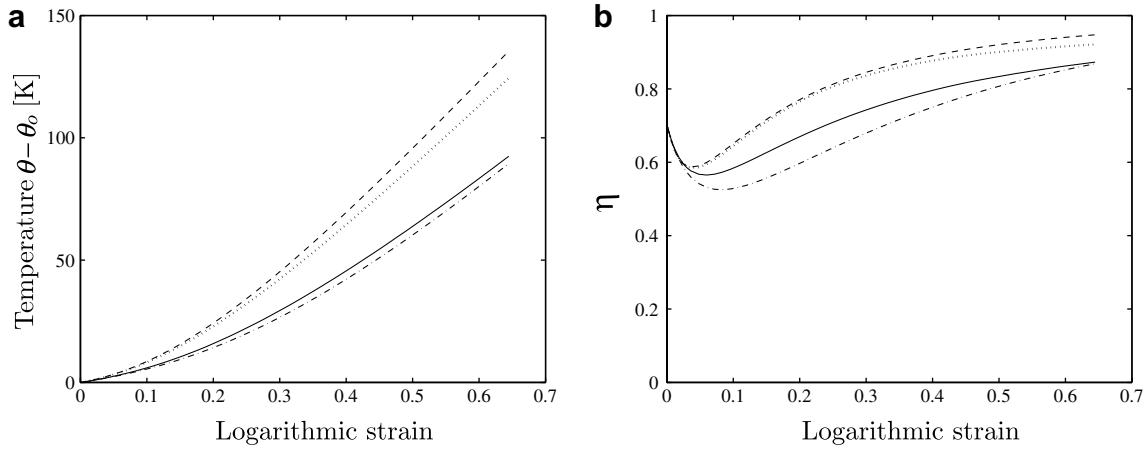

Fig. 7. Uniaxial thermal response for modeling different initial distributions of the crystal orientations: (a) temperature evolution, (b) η, fraction of the plastic work dissipated as heat. Goss distribution – solid line, Brass distribution – dashed line, single crystal – dashed-dotted line, isotropic distribution – dotted line.

conditions as in the previous example, an isotropic distribution of 400 grains being used within each integration point. The specimen is loaded in the RD-direction using a triangular cyclic strain history with a logarithmic strain amplitude of 0.05 and a rate of 0.1 s^{-1}. The mechanical response is shown in Fig. 8a and the temperature evolution in Fig. 8b, where the effects of both the isotropic and the kinematic hardening can be seen. The change in the initial isotropic orientation of the crystals is almost unaffected by the deformation. The deformations in this example are considerably smaller than in the previous case, where the texture evolution was more prominent. Since the small deformations together with the cyclic deformation do not result in any plastic spin, a clear texture does not develop.

The heat generation in the form of mechanical dissipation together with the rate of stored energy, are presented in Fig. 9. The rate of stored energy is equal to the difference between the dissipation and the rate of plastic work. Note that at the onset of reversed plastic flow the rate of stored energy becomes negative, which means that the heat generation is greater than the rate of plastic work. The η-factor as defined in (25) then become greater than 1. This effect was noted for a pure kinematic hardening model by Chaboche (1993), who concluded that during uniaxial reversed plasticity the rate of stored energy is negative until the backstress has changed sign. Part of the energy stored during the first half cycle is released during the second half

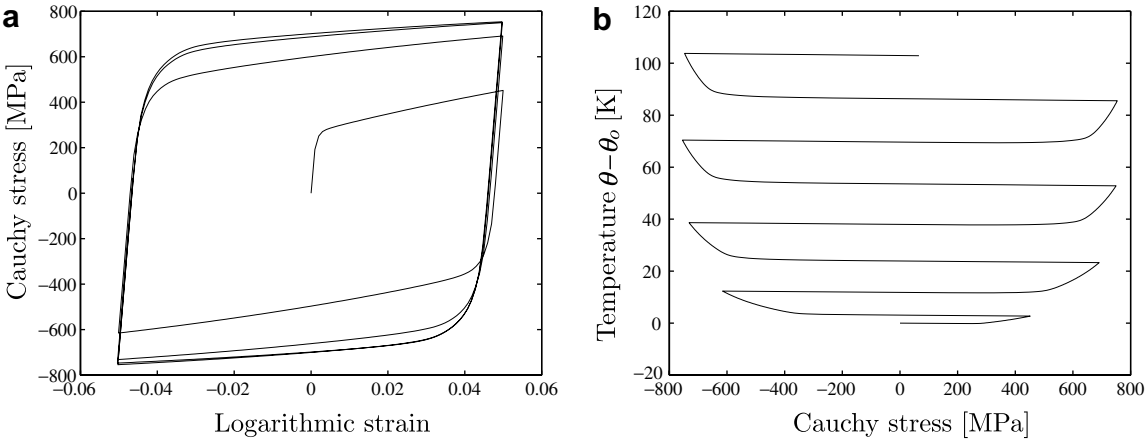

Fig. 8. Uniaxial cyclic response, with a strain amplitude of 0.05: (a) mechanical response, (b) temperature evolution.

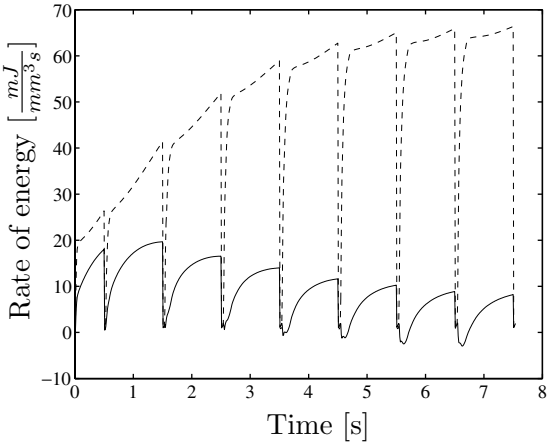

Fig. 9. The solid line represents the rate of stored energy and the dashed line represents the mechanical dissipation. The quantities are given as the rate of energy per unit volume in the current configuration.

cycle and is converted to heat, or in extreme cases to mechanical work. This phenomena has been verified experimentally by Dillon (1966), who measured the rate of stored energy during the cyclic torsional loading of copper tubes. It can be concluded that it is not suitable in the case of cyclic loading to base the heat generation on a fraction of the rate of plastic work defined as $w^{\mathrm{p}} = \boldsymbol{\Sigma} : \boldsymbol{I}^{\mathrm{p}}$ for large deformations and as $w^{\mathrm{p}} = \sigma : \dot{\epsilon}^{\mathrm{p}}$ for small deformations. If the heat generation is assumed to be a constant fraction of the rate of plastic work, the heat generation during reversed plastic flow would be too small. In the extreme case in which reversed plastic flow takes place before loading has changed direction, the heat generation could even be negative.

4.3. Cyclic loading of Cook's membrane

The last example to be considered involves cyclic loading of Cook's membrane. The same geometry as in Håkansson et al. (2005) is used. The dimensions are shown in Fig. 10a, in which $H_1 = 44$ mm, $H_2 = 16$ mm and $L = 48$ mm. The membrane is modeled by 360 four-node fully integrated plane strain elements, cf. Fig. 10b. In contrast to the simulation reported in Håkansson et al. (2005), the membrane here is loaded with a prescribed displacement u as shown in Fig. 10a. The right-hand side of the structure is clamped so that the prescribed displacement can be applied to a single point. The prescribed displacement is described by a sinusoidal function $u = 2.5 \sin\left(\frac{2\pi}{5} t\right)$ mm, where t is the time in seconds. In the simulation, 400 isotropic distributed crystals are used per integration point.

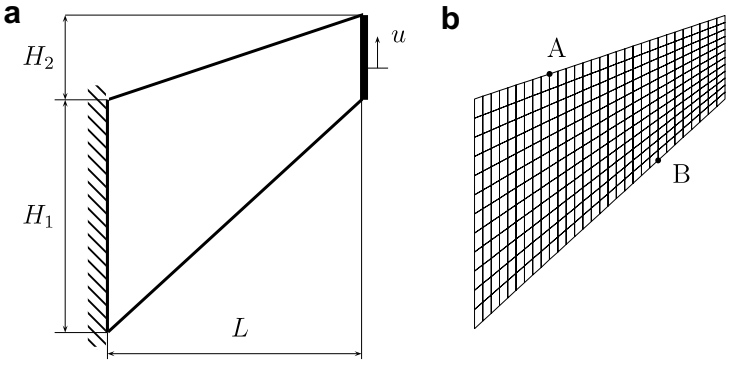

Fig. 10. Cook's membrane: (a) the geometry; (b) the mesh.

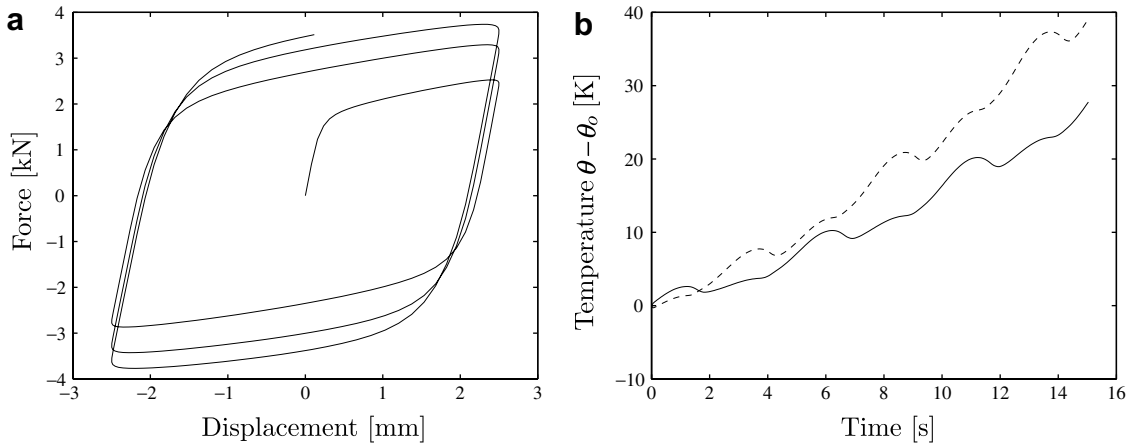

Fig. 11. Cyclic response of Cook's membrane: (a) mechanical response; (b) temperature evolution versus time, the solid line corresponding to point A and the dashed one to point B, cf. Fig. 10b.

The mechanical and the thermal response are presented in Fig. 11. In Fig. 11b there is a temperature dip in each load cycle, the temperature dips being due to the Kelvin effect, which is described by the last term in (A.5). The Kelvin effects is driven by a change in volume, an increase in volume yielding a decrease in temperature. The temperature dips in Fig. 11b thus take place after the loading direction has changed but before the mechanical dissipation becomes greater than the Kelvin effect. Experimentally measured temperature variations due to the Kelvin effect during cyclic uniaxial loading has been done by Boulanger et al. (2004). The temperature variations in Fig. 11b agrees fairly well with the findings in Boulanger et al. (2004), the measured effect is, however, slightly less pronounced which can be traced to a small difference in the specific heat and to the assumed adiabatic conditions. In this numerical example the temperature changes are, compared to a

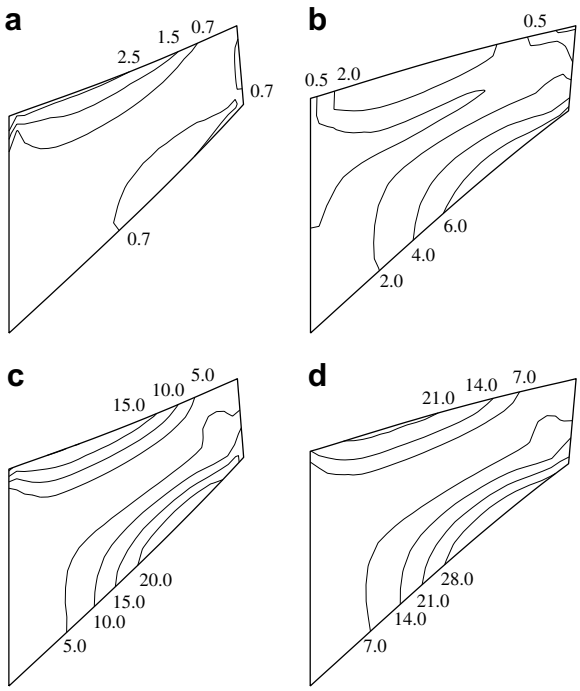

Fig. 12. Relative temperature distribution [K]. The specific times are (a) 1.25 s, (b) 3.75 s, (c) 11.25 s and (d) 13.75 s.

physical test or a fully coupled thermomechanical simulation, slightly larger due to the absence of heat conduction and heat convection, cf. Håkansson et al. (2005).

The temperature distribution at the maximum and the minimum of the displacement described is shown in Fig. 12 for the first and the last cycle. As can be seen in Fig. 11b, the largest plastic development takes place around the lower edge of the membrane, where the temperature evolution is higher for point B than for point A. As discussed in connection with the example involving uniaxial cyclic loading, the deformations in Cook's membrane are too small to give rise to a significant texture evolution. The loading situation differs from uniaxial cyclic loading in the respect that Cook's membrane is analyzed with the assumption of plane strain.

5. Conclusions

The heat generation properties of polycrystalline materials with different initial textures were studied here. The investigations were conducted on aggregates consisting of 400 grains, the behavior of each grain being described by a single crystal plasticity model. The homogenization of the aggregates was carried out using the Taylor average scheme.

The single crystal model used to describe the polycrystal behavior involved is a rate-dependent model formulated within a thermodynamic framework for large strains. The modeling of the slip resistance and the choice of evolution laws for the internal variables related to the slip resistance turned out to be crucial to the dissipation inequality being fulfilled and a heat generation being obtained that agreed with results of experimental tests. The slip resistance was modeled in accordance with Busso and Cailletaud (2005), in which the latent-hardening is included on a total form in the Helmholtz free energy function, which was complemented by evolution laws of Armstrong–Frederick type which are local for each slip system.

In the first numerical example, which concerns the uniaxial loading of a material with an isotropic initial crystal orientation distribution, it was found to be possible to mimic the heat generation obtained in experimental tests. The comparison between the adiabatic and the isothermal results showed the mechanical response to be highly temperature-dependent, confirming that the temperature effect cannot be neglected if accurate results are to be obtained at high loading rates. For the uniaxial examples with different initial textures it could be concluded that the different initial textures result in significantly different mechanical and thermal response. Perhaps the most interesting finding was that the initial texture had a strong influence on the heat conversion factor. The difference between the single crystal and the texture based on the Goss distribution was particularly notable, the rate of stored energy was larger for the single crystal than for the Goss distribution. Since the orientation of the single crystal and the Goss orientation component are equivalent in the specific loading case the difference in the rate of stored energy can be found in the randomized distribution.

The heat generation during cyclic uniaxial loading was also investigated, the study involved use of a material with an initially isotropic crystal orientation distribution. It was shown that for a material displaying a Bauchinger effect the formulation of the mechanical dissipation is extremely important. The heat generation cannot readily be based on the rate of plastic work, defined as $w^{\mathrm{p}} = \boldsymbol{\Sigma} : \boldsymbol{l}^{\mathrm{p}}$, since during reversed plastic flow that quantity is too small or is even negative.

The last example was that of the cyclic loading of Cook's membrane the capabilities of the model for dealing with a large finite element problem was here demonstrated.

Appendix A. Integration of the constitutive equations

The simulation of polycrystalline material, which can consist of up to hundreds of thousands crystals, is computationally very costly. A effective integration of the constitutive equations is thus called for. The numerical examples presented in the paper were analyzed under adiabatic conditions, which means that instead of solving a fully coupled thermomechanical problem, in which the mechanical field equation and the heat equation are solved simultaneously (or using a staggered method) the temperature is a local quantity. The evolution of the local temperature is accounted for by the stress-updating procedure. Exponential mapping is used to integrate the rate of the plastic deformation gradient in (2), cf. Weber and Anand (1990), Steinmann and Stein (1996). One of the advantages of an exponential map is that the isochoric properties of the plastic deformation are preserved. The plastic deformation gradient in the updated state $n+1$ can be expressed as

$$\boldsymbol{F}^{\mathrm{p}}_{n+1} = \exp(\Delta t \boldsymbol{l}^{\mathrm{p}}_{n+1})\boldsymbol{F}^{\mathrm{p}}_{n} \tag{A.1}$$

where Δt is the time step between state $n+1$ and the last equilibrium state n. Since $\boldsymbol{l}^{\mathrm{p}}_{n+1}$ is only dependent upon $\Delta\gamma^{\alpha}$, cf. (13), the recoverable deformation tensor in state $n+1$ can be explicitly expressed as

$$\boldsymbol{C}^{\mathrm{r}}_{n+1} = \exp(-\Delta t \boldsymbol{l}^{\mathrm{p}}_{n+1})^{\mathrm{T}}\, \widetilde{\boldsymbol{C}}^{\mathrm{r}} \exp(-\Delta t \boldsymbol{l}^{\mathrm{p}}_{n+1}) \tag{A.2}$$

where $\widetilde{\boldsymbol{C}}^{\mathrm{r}} = (\boldsymbol{F}^{\mathrm{p}}_{n})^{-T}\boldsymbol{F}^{\mathrm{T}}_{n+1}\boldsymbol{F}_{n+1}(\boldsymbol{F}^{\mathrm{p}}_{n})^{-1}$. To calculate the exponential tensor in an efficient manner use is made of a first-order Padé approximation, i.e. $\exp(\boldsymbol{A}) = (\boldsymbol{1} - \frac{1}{2}\boldsymbol{A})^{-1}(\boldsymbol{1} + \frac{1}{2}\boldsymbol{A})$. The internal quantities that controls the slip resistance and the back-stress are integrated with a backward-Euler scheme, i.e.

$$g^{\alpha}_{n+1} = g^{\alpha}_{n} + \Delta g^{\alpha} \tag{A.3}$$

$$v^{\alpha}_{n+1} = v^{\alpha}_{n} + \Delta v^{\alpha} \tag{A.4}$$

Using the evolution law (19) and the integration scheme in (A.4), i.e. $\Delta v^{\alpha} = \Delta\gamma^{\alpha} - R v^{\alpha}_{n+1}|\Delta\gamma^{\alpha}|$, Δv^{α} can be explicitly expressed as a function of $\Delta\gamma^{\alpha}$. It is not possible, however, to obtain a corresponding expression for Δg^{α}. Since the model is used in an adiabatic simulation it is suitable to include the temperature evolution in the integration of the constitutive equations. After the parts of the heat equation (5) belonging to the heat conduction and the external heat source have been excluded, the remaining evolution for the temperature can be expressed as

$$\rho_0 c \Delta\theta = (\gamma_{\mathrm{mech}})_{n+1}\Delta t + \rho_0(\theta \partial_{\theta \boldsymbol{J}}\psi)_{n+1}\Delta t \tag{A.5}$$

The temperature is integrated using a backward-Euler scheme, i.e. $\theta_{n+1} = \theta_n + \Delta\theta$. From (A.5) an explicit expression for $\Delta\theta$ dependent only on $\Delta\gamma^{\alpha}$ and Δg^{α} can be obtained. The temperature thus does not require that any additional equations be solved. The remaining equations that need to be solved are (15) and (20), which leads to the following system of equations, all quantities being evaluated in the state $n+1$

$$\begin{aligned} \mathcal{R}^{\alpha}_{\gamma} &= \Delta\gamma^{\alpha} - \Delta t\dot{\gamma}_0\left(\frac{|\tau^{\alpha} - b^{\alpha}|}{G^{\alpha}_{r}}\right)^{m}\operatorname{sgn}(\tau^{\alpha} - b^{\alpha}) = 0 \\ \mathcal{R}^{\alpha}_{g} &= \Delta g^{\alpha} - \frac{|\tau^{\alpha} - b^{\alpha}|}{G^{\alpha}_{r}}(1 - B g^{\alpha})|\Delta\gamma^{\alpha}| = 0 \end{aligned} \tag{A.6}$$

The system of non-linear equations, two equations per slip system, is solved by a Newton–Raphson method. The independent solution variables are collected in the matrix $\boldsymbol{Y} = [\Delta\gamma^1 \Delta g^1 \cdots \ \Delta\gamma^n \Delta g^n]$.

Appendix B. Linearization of the constitutive equations

In the finite element program a linearization of the second Piola–Kirchhoff stress tensor, $\boldsymbol{S}$, with respect to the Green–Lagrange strain tensor, $\boldsymbol{E}$, is needed. The algorithmic stiffness tensor, defined as $\mathrm{d}\boldsymbol{S} = \boldsymbol{D}^{\mathrm{ATS}}{:}\mathrm{d}\boldsymbol{E}$, can be calculated from

$$\boldsymbol{D}^{ATS} = 4\rho_0 \frac{\mathrm{d}}{\mathrm{d}\boldsymbol{C}}\left((\boldsymbol{F}^{\mathrm{p}})^{-1}\frac{\partial\psi}{\partial\boldsymbol{C}^{\mathrm{r}}}(\boldsymbol{F}^{\mathrm{p}})^{-T}\right) \tag{B.1}$$

where all the quantities are calculated in state $n+1$. The inverse of the plastic deformation gradient is differentiated using (A.1), i.e.

$$\frac{\mathrm{d}(\boldsymbol{F}^{\mathrm{p}})^{-1}}{\mathrm{d}\boldsymbol{C}} = (\boldsymbol{F}^{\mathrm{p}}_{n})^{-1}\sum_{\alpha=1}^{n}\frac{\mathrm{d}}{\mathrm{d}\Delta\gamma^{\alpha}}(\exp(-\Delta t\boldsymbol{l}^{\mathrm{p}}))\otimes\frac{\mathrm{d}\Delta\gamma^{\alpha}}{\mathrm{d}\boldsymbol{C}} \tag{B.2}$$

The differentiation of the exponential tensor follows directly from the Padé approximation. In the differentiation of $\Delta\gamma^{\alpha}$, the derivatives of $\boldsymbol{Y}$ with respect to $\boldsymbol{C}$ are needed. These can be calculated by a method used by Ekh and Runesson (2001) and Håkansson et al. (2005). The system of equations in (A.6) which is completely determined by the variables in $\boldsymbol{Y}$ and $\widetilde{\boldsymbol{C}}^{\mathrm{r}}$ can be summarized as $\boldsymbol{\mathcal{R}}(\boldsymbol{Y}(\widetilde{\boldsymbol{C}}^{\mathrm{r}}),\ \widetilde{\boldsymbol{C}}^{\mathrm{r}}) = \boldsymbol{0}$, where $\boldsymbol{\mathcal{R}}$ is a collection of the residuals in (A.6), i.e. $\boldsymbol{\mathcal{R}} = [\mathcal{R}^1_{\gamma}\ \mathcal{R}^1_{g}\cdots\mathcal{R}^n_{\gamma}\ \mathcal{R}^n_{g}]$. A differentiation yields

$$\frac{\mathrm{d}\boldsymbol{Y}}{\mathrm{d}\widetilde{\boldsymbol{C}}^{\mathrm{r}}} = -\left[\frac{\partial \boldsymbol{\mathcal{R}}}{\partial \boldsymbol{Y}}\right]^{-1} \frac{\partial \boldsymbol{\mathcal{R}}}{\partial \widetilde{\boldsymbol{C}}^{\mathrm{r}}} \tag{B.3}$$

This makes it possible to calculate the derivatives of the independent variables as

$$\frac{\mathrm{d}\boldsymbol{Y}}{\mathrm{d}\boldsymbol{C}} = \frac{\mathrm{d}\boldsymbol{Y}}{\mathrm{d}\widetilde{\boldsymbol{C}}^{\mathrm{r}}} : \frac{\mathrm{d}\widetilde{\boldsymbol{C}}^{\mathrm{r}}}{\mathrm{d}\boldsymbol{C}} \tag{B.4}$$

The remaining difficulties in (B.1) involve the determination of $\frac{\partial^2 \psi}{\partial \boldsymbol{C}^{\mathrm{r}} \partial \boldsymbol{C}^{\mathrm{r}}}$, where due to the logarithmic form of the Helmholtz free energy the differentiation involves derivatives of the eigenvalues and the eigenvectors of $\boldsymbol{C}^{\mathrm{r}}$. A description of this procedure can be found in Simo and Taylor (1991) and Miehe (1998).

B.1. Remark

In the description of the algorithmic stiffness tensor above, adiabatic conditions were assumed. However, if the proposed model is to be used in a coupled thermomechanical simulation, the linearization of the second Piola–Kirchhoff stress tensor is slightly different, the stress tensor needs to also be differentiated with respect to the temperature, i.e.

$$\mathrm{d}\boldsymbol{S} = \boldsymbol{D}^{ATS} : \mathrm{d}\boldsymbol{E} + \boldsymbol{D}^{\theta}\mathrm{d}\theta \tag{B.5}$$

In this situation, the temperature evolution (A.5) is of course not included in the stress integration.

References

Anand, L., 2004. Single-crystal elasto-viscoplasticity: application to texture evolution in polycrystalline metals at large strains. Comput. Methods Appl. Mech. Engng. 193, 5359–5383.

Anand, L., Balasubramanian, S., Kothari, M., 1997. Constitutive modeling of polycrystalline metals at large strains. In: Teodosiu, C. (Ed.), The Constitutive Law in Thermoplasticity. CISM Courses and Lectures No. 376. Springer-Verlag, Udine, pp. 109–172.

Andrade-Campos, A., Teixeira-Dias, F., Gràcio, J., 2005. Modelling the effect of strain rate on the thermomechanical behaviour of AISI 304 stainless steel. Mat. -wiss. u Werkstofftech. 36, 566–571.

Benzerga, A., Brechet, Y., Needleman, A., Van der Giessen, E., 2005. The stored energy of cold work: predictions from discrete dislocation plasticity. Acta Mater. 53, 4765–4779.

Bodner, S., Partom, Y., 1975. Constitutive equations for elastic-viscoplastic strain hardening materials. J. Appl. Mech. Trans. ASME 42, 385–389.

Borg, U., 2007. A strain gradient crystal plasticity analysis of grain size effects in polycrystals. Eur. J. Mech. A/Solids. 26, 313–324.

Boulanger, T., Chrysochoos, A., Mabru, C., Galtier, A., 2004. Calorimetric analysis of dissipative and thermoelastic effects associated with the fatigue behavior of steel. Int. J. Fatigue 26, 221–229.

Busso, E., Cailletaud, G., 2005. On the selection of active slip systems in crystal plasticity. Int. J. Plasticity 21, 2212–2231.

Chaboche, J.L., 1993. Cyclic viscoplastic constitutive equations, part I: a thermodynamically consistent formulation. J. Appl. Mech. 69, 813–821.

Chen, X., Wang, Y., Ming, G., Yuanming, X., 2004. Dynamic behavior of SUS304 stainless steel at elevated temperatures. J. Mater. Sci. 39, 4869–4875.

Clayton, J., 2005. Dynamic plasticity and fracture in high density polycrystals: constitutive modeling and numerical simulation. J. Mech. Phys. Solids 53, 261–301.

Dillon, O., 1966. The heat generated during the torsional oscillations of copper tubes. Int. J. Solids Struct. 2, 181–204.

Ekh, M., Runesson, K., 2001. Modeling and numerical issues in hyperelasto-plasticity with anisotropy. Int. J. Solids Struct. 38, 9461–9478.

Franciosi, P., 1985. The concepts of latent hardening and strain hardening in metallic single crystal. Acta Metall. 33, 1601–1612.

Håkansson, P., Wallin, M., Ristinmaa, M., 2005. Comparison of isotropic hardening and kinematic hardening in thermoplasticity. Int. J. Plasticity 21, 1435–1460.

Hill, R., 1966. Generalized constitutive relations for incremental deformation of metal crystals by multislip. J. Mech. Phys. Solids 14, 95–102.

Horstemeyer, M., McDowell, D., McGinty, R., 1999. Design of experiments for constitutive model selection: application to polycrystal elastoviscoplasticity. Modell. Simulat. Mater. Sci. Engng. 7, 253–273.

Hutchinson, J., 1970. Elastic–plastic behaviour of polycrystalline metals and composites. Prog. Mater. Sci. 319, 247–272.

Hutchinson, J., 1976. Bounds and self-consistent estimates for creep of polycrystalline materials. Proc. R. Soc. Lond. A. 348, 101–127.

Kocks, U., Tomé, C., Wenk, H.-R., 1998. Texture and Anisotropy Preferred, Orientations in Polycrystals and Their Effect on Materials Properties. Cambridge University Press.

Kröner, E., 1960. Allgemeine kontinuumstheorie der versetzungen. Arch. Rat. Mech. Anal., 273–334.

Kuroda, M., Tvergaard, V., 2007. Effects of texture on shear band formation in plane strain tension/compression and bending. Int. J. Plasticity 23, 244–272.
Lee, E.H., 1969. Elastic–plastic deformation at finite strains. J. Appl. Mech. 36, 1–6.
Mandel, J., 1971. Plasticite Classique et Viscoplasticity. CISM Course No. 97. Springer-Verlag, Udine.
Méric, L., Poubanne, P., Cailletaud, G., 1991. Single crystal modeling for structural calculations: Part 1 – model presentation. J. Engng. Mater. Technol. 13, 162–170.
Miehe, C., 1998. Comparison of two algorithms for the computation of fourth order isotropic tensor functions. Comput. Struct. 66, 37–43.
Miehe, C., Schröder, J., Schotte, J., 1998. Computational homogenization analysis in finite plasticity simulation of texture development in polycrystalline materials. Comput. Methods Appl. Mech. Engng. 171, 387–418.
Morabito, A.E., Chrysochoos, A., Dattoma, V., Galietti, U., 2007. Analysis of heat sources accompanying the fatigue of 2024 T3 aluminium alloys. Int. J. Fatigue 29, 977–984.
Nemat-Nasser, S., Okinaka, T., 1996. A new computational approach to crystal plasticity: Fcc single crystal. Mech. Mater. 24, 43–57.
Ohashi, T., 2004. Three dimensional structures of the geometrically necessary dislocations in matrix-inclusion systems under uniaxial tensile loading. Int. J. Plasticity 20, 1093–1109.
Oliferuk, W., Maj, M., 2004. Effect of pre-strain direction on energy storage process during tensile deformation of polycrystal. Mater. Sci. Eng. 387–389, 218–221.
Oliferuk, W., Swiatnicki, W., Grabski, M., 1993. Rate of energy storage and microstructure evolution during the tensile deformation of austenitic steel. Mater. Sci. Eng. A 161, 55–63.
Peirce, D., Asaro, R., Needleman, A., 1982. An analysis of nonuniform and localized deformation in ductile single crystals. Acta Metall. 30, 1087–1119.
Peirce, D., Asaro, R., Needleman, A., 1983. Material rate dependence and localized deformation in crystalline solids. Acta Metall. 31, 1951–1976.
Piercy, G.R., Cahn, R.W., Cottrell, A.H., 1955. A study of primary and conjugate slip in crystals of alpha-brass. Acta Metall. 55, 331–338.
Rice, J., 1971. Inelastic constitutive relations for solids: an internal-variable theory and its application to metal plasticity. J. Mech. Phys. Solids 19, 433–455.
Ristinmaa, M., Wallin, M., Ottosen, N.S., 2007. Thermodynamic format and heat generation of isotropic hardening plasticity. Acta Mech 194, 103–121.
Rosakis, P., Rosakis, A., Ravichandran, G., Hodowany, J., 2000. A thermodynamic internal variable model for the partition of plastic work into heat and stored energy in metals. J. Mech. Phys. Solids 48, 581–607.
Simo, J.C., Taylor, R.L., 1991. Quasi-incompressible finite elasticity in principle stretches. Continuum basis and numerical algorithms. Comput. Methods Appl. Mech. Engng. 85, 273–310.
Steinmann, P., Stein, E., 1996. On the numerical treatment and analysis of finite deformation ductile single crystal plasticity. Comput. Methods Appl. Mech. Engng. 129, 235–254.
Tavassoli, A., 1995. Assessment of stainless steels. Fus. Eng. Des. 29, 371–390.
Taylor, G., 1938. Plastic strain in metals. J. Inst. Met. 62, 307–324.
Taylor, G., Quinney, H., 1934. The latent energy remaining in a metal after cold working. Prog. Mater. Sci. A 143, 307–326.
Weber, G., Anand, L., 1990. Finite deformation constitutive equations and a time integration procedure for isotropic, hyperelastic-viscoplastic solids. Comput. Methods Appl. Mech. Engng. 79, 173–202.